The Limaçon of Pascal - Mechanical Generation and Utilisation for Fluid Processing

Ibrahim A. Sultan
School of Science and Engineering
The University of Ballarat
PO Box 663
Ballarat 3353 VICTORIA, Australia
Email: i.sultan@ballarat.edu.au

ABSTRACT

The limaçon of Pascal is a plane curve that possesses some characteristics which qualify it for fluid processing applications. However, the curve has not yet attracted enough attention, neither from industry nor from the mechanical engineering research community, despite the few attempts that have been conducted over the past century. The work presented here is intended to explore various mechanical linkages that can be employed to produce the limaçon, and the aspects of these linkages. Mathematical analysis will show that machines based on the limaçon curve possess sinusoidal volumetric relationships and hence simplified pressure and torque equations can be obtained in closed forms. The concepts discussed here will be demonstrated by using a compressor as a sample application.

Keywords: limaçon, compressor, expander, mechanism, instant centre, pressure, torque, volumetric efficiency, rotary, Wankel.

NOTATION

θ	angle of rotation
L	half the length of cord
r	radius of the base circle
s	sliding distance
ψ	crank rotation

p1	point of the limaçon chord
p2	point on the limaçon chord
m	centre point of chord
o	pole of limaçon
c	centre of the base circle
I	instantaneous centre of rotor
R	polar representation of the limaçon
R_m	limaçon radius measured from blank centre
x	the x-coordinate of p1 w.r.t. the pole
y	the y-coordinate of p1 w.r.t. the pole
X_m	the x-coordinate of p1 w.r.t. the blank centre
Y_m	the y-coordinate of p1 w.r.t. the blank centre
A_t	area above chord
A_b	area below chord
A_{tot}	total limaçon area
A_{id}	difference between A_t and A_b.
H	rotor depth
V_t	volume above chord
V_b	volume below chord
V_{max}	maximum chamber volume
V_{min}	minimum chamber volume
V_{id}	induced volume per half a revolution
P_1	pressure during isentropic compression
P_i	inlet pressure
P_d	delivery pressure
P_2	pressure during isentropic expansion
P_{at}	atmospheric pressure
T_1	fluid torque during isentropic compression
T_2	fluid torque during scavenging

T_3 fluid torque during isentropic expansion

T_4 fluid pressure during induction

β rotor angle when discharge valve opens

α rotor angle when inlet valve opens

C_r compression ratio

γ specific heat ratio

η_v volumetric efficiency

1. INTRODUCTION

The limaçon is an interesting plane curve that has been investigated by mathematicians as far back as the 16th century. It was named, as Costa et al (1999) point out, after Etienne Pascal, father of the well known French scientist Blaise Pascal. The curve is qualified by its mathematical characteristics to be used for rotary fluid processing machines such as pumps, compressors, motors and engines. However, it has not attracted attention from industry as reflected by the accounts, of various designs currently used for rotary fluid processing, listed by Yamamoto (1981) and Artobolvesky (1983).

Currently, most of the industrial and research effort in the area of rotary compression-expansion machinery is directed towards improving the performance of existing technology, which features, among other things, screw-, vane- and gear-type equipment. The screw fluid processing concept has gained particular popularity in industry and attracted a considerable amount of research effort. Mimmi and Pennacchi (1999) present an example of such effort as they perform a geometric analysis of a twin-screw three-lobed blower with a modified lobe contour. Tong and Yang (2000) present an investigation of the effects of the lobe geometry on the flow capacity of a two-lobe pump; they, therefore, propose an elegant mathematical technique to design lobe pumps with improved flow characteristics. Machines which employ a two-lobe and three-lobe straight rotors are referred to as the “Roots” and their thermodynamic characteristics are

explained by Eastop and McConkey (1996). However, Peng et al (2002) suggest that such arrangements are inefficient when used for gas handling due to the lack of built-in compression, and, alternatively, they present a compressor which features two parallel rotors in a casing, whereby each rotor is equipped with a single tooth to create variable volume entrapped between the two teeth and the inner surface of the casing. A limaçon fluid processing machine can readily be equipped with built-in pressure characteristics, and as such they are likely to be more efficient than the Roots. Ertesvag (2002) develops geometric and thermodynamic models for a novel vane-type machine, which features a rotor (carrying radial vanes) positioned eccentrically in a cylindrical casing. The vanes were made to slide, in and out, during rotations to create variable volume chambers suitable for fluid processing. In this vane-type design the vanes did not touch the inner surface of the housing by virtue of a mechanical arrangement.

Many rotary machines, currently used in industry, employ casings whose inner surfaces are made out of either perfect circular cross sections, or circular-arc sections. However, Yamamoto (1981) dedicates his work to a noticeable exception; which is the rotary engine (also known as the Wankel engine) that uses a three-sided rotor, and housing made out of an epitrochoidal curve produced by an epicycloidal gear train. Interestingly a few years before Wankel patented his rotary design in 1936, Planche (1920 and 1927) had employed the same epicycloidal gear train to produce a fluid processing device. However, unlike Wankel, Planche proportioned his gear train to produce limaçon motion.

In fact attempts to produce compression-expansion machines based on the limaçon motion can be traced back to a US patent by Wheildon (1896); such work that was later rediscovered by Georgiev (1981), where considerable improvements have been made to the design. Examples of other efforts that were intended to produce the same motion, using various mechanical transformations, may be found in patents by Feyens (1927), Frager and Menard (1962) and Campo (1919). However, most of the proposed prototypes were built with circular housing instead of a proper limaçon (Georgiev's device may have been an exception), and not enough attention was given to the rotor profile. This may be attributed either to inventors being unaware of the nature of the proper housing curve or to manufacturing difficulties; and it would result in considerable

reduction to various efficiency figures, which may justify the fact that none of these machines, despite their considerable potential, has found its way to industrial-scale production. However, with the progress currently achieved in manufacturing technology, it is expected that accurately machined limaçon housings will now be more producible than they have ever been.

2. KINEMATICAL BACKGROUND

The limaçon can be obtained by modifying the Nicodemes choncoidograph (Costa et al, 1999) in such a way that the base of the conchoid is a circle, whereby the pole of conchoid falls on its circumference. As such, Artobolevsky (1964) presents the mechanism shown in Figure (1) as a simple system that can be employed to produce limaçon motion. The arrangement creates a limaçon by tracing the path of any point on the chord ($\overline{p1p2}$), at a distance L from a rotating point, m (which also falls on the chord). The chord must always pass by the pole (i.e. point o) as point m performs uniform rotations on a base circle, whose radius is r. The two points on the chord at the same distance on either side of the rotating point, m, fall on the same limaçon. In fluid processing applications, point m is a centre point on the rotor lateral axis where the endpoints, p1 and p2, fall at a distance L from this centre. The produced limaçon is the curve describing the inner surface of a compression-expansion chamber. Figure (2) depicts the mechanism shown in Figure (1) as it has been employed for a fluid processing machine. As point m negotiates its circular path, the area subtended between the limaçon and the rotor lateral axis varies with the angle of rotation, θ. This variation is consequently employed to effect the compression-expansion action.

Some aspects of the limaçon mechanism could be concluded by inspecting Figure (1);

i. Because both points, o and m, fall on the same base circle, the rotor angle, θ, is always equal to half the central angle, ψ. Hence, the rotor lateral axis rotates at half the angular velocity of its centre, m.

ii. As the rotor lateral axis performs half a revolution, the end points, p1 and p2, trace opposite portions on the limaçon, in such a way that the whole chamber

is swept by each side of the rotor during this half-revolution. However, whilst one side is inducing fluid into the chamber, the other would be performing a scavenging stroke. In other words, a limaçon fluid processing device is a double-acting machine, which produces two simultaneous compression-expansion cycles during a single driveshaft revolution. However for this to be realised, the driveshaft must be aligned with the pole, o, rather than the base circle centre. Various alternative designs of the limaçon mechanism are demonstrated in the next section.

iii. In accordance with the Kennedy-Aronholdt theorem (Waldron and Kinzel, 1999), the instantaneous centre, I, of the rotor always falls on the base circle diametrically opposite the centre point, m. As such the base circle is actually the fixed centrode of the limaçon chord (and hence the rotor), and I is the centre of curvature of the limaçon. In fact, the base circle is the common evolute for all limaçons developed of the same chord; and they all share the same centre of curvature at any given angle of rotation, θ.

Kinematically, it is worth noting that the specific mechanism used for demonstration, in Figure (1), suffers from a singularity at the position $\theta = 0$. At this position, the two lines, $\overline{mI}$ and $\overline{oI}$, whose intersection defines the instantaneous centre, I, would coincide indicating a vanishing system Jacobian. Hence, a momentary loss of the proper instantaneous centre will occur, causing the housing to start supporting the rotor apices to guide them back in the tangent direction. This should be avoided since it results in noise and accelerated wear, particularly at low speed applications. Artobolevsky (1964) employs a rhomboid-shaped four-bar linkage to generate the limaçon. However this mechanism, besides being too involved to use in fluid processing, represents a Class-III kinematic chain which also suffers singularity at the position where all links collapse to a single straight line. Fortunately, not all versions of the limaçon mechanism suffer from singularity as the examples given in the next section will show. All the mechanisms demonstrated in this section are non-singular and do not rely on the housings to perform their motions.

iv. The moving centrode of the rotor is defined by the path of point I with respect to a coordinate system rigidly attached to the rotor body. In Figure (1), XrYr is a coordinate system attached to the chord (which is the rotor axis) at its centre point, m. As the distance mI is always equal to a constant value of 2r, the moving centrode is a circle whose centre is m and whose diameter is twice that of the base circle. Since the moving centorde performs a pure rolling motion on the fixed centrode (whereby I is the contact point), a definition of the limaçon is revealed. It is a curve produced by a point attached to a circle, whose radius is 2r, as it performs epicycloidal rolling motion on a fixed circle whose radius is r.

v. The maximum value of the sliding motion, s, is equal to diameter of base circle.

With the origin of a ground XY-coordinate system situated at the pole, o, as shown in Figure (1), the instantaneous sliding distance, s of the rotor can be expressed as follows;

$$s = 2r\sin(\theta) \tag{1}$$

where r is the radius of the base circle and θ is half the angle rotated by the crank from the initial vertical position. The radial distance R of p1 with respect to the pole, o, is given as follows;

$$R = 2r\sin(\theta) + L \tag{2}$$

where L is half the rotor width. Equation (2) reveals that the portions of the limaçon housing profile which fall above the x-axis, and which are bounded by $0 \le \theta \le \pi/2$ and $\pi/2 \le \theta \le \pi$, are symmetrical about the y-axis. Likewise, the portions of the limaçon which fall bellow the x-axis, and which are bounded by $\pi \le \theta \le 3\pi/2$ and $3\pi/2 \le \theta \le 2\pi$ are symmetrical about the y-axis. It may then be concluded that the limaçon curve is symmetrical about the y-axis.

The x- and y- coordinates of p1 can then be expressed as follows;

$$x = r\sin(2\theta) + L\cos(\theta) \tag{3}$$

and

$$y = r - r\cos(2\theta) + L\sin(\theta) \tag{4}$$

For the limaçon to be employable as a compression-expansion machine, it should possess a looping- and dimple-free profile (mathematically, this is referred to as an ordinary limaçon). Costa et al (1999) offer a discussion, albeit in an abstract mathematical sense, on how the curve parameters affect its convexity and curvature. Based on this discussion, for a fluid processing limaçon the following relationship should hold;

$$r / L \leq 0.25 \tag{5}$$

This relationship agrees with what has been suggested by Artobolevsky (1964), Hunt (1978) and Georgiev (1981), and it indicates that points, p1 and p2, must not fall inside a circle whose centre is m and whose radius is twice the radius of the moving centrode for the limaçon to be suitable for fluid processing. This circle may be referred to, in the context of the work presented here, as the critical circle of the limaçon.

Keeping in mind that (5) ensures that the compression-expansion limaçon would be a single-looped continuous contour, and taking (2) into account, it could be concluded that the highest and lowest points on the limaçon are respectively at distances of L+2r and L-2r vertically above and below the pole, o. This suggests that the geometric centre of the circular blank, of which the housing would be machined, should fall on the base circle at a point diametrically opposite the pole, o. As such the machining equations, which describe the x- and y- coordinates of the limaçon with respect to the work piece centre, may be expressed as follows;

$$X_m = r\sin(2\theta) + L\cos(\theta) \tag{6}$$

and

$$Y_m = -r - r\cos(2\theta) + L\sin(\theta) \tag{7}$$

These last two equations (6) and (7) can be combined to produce the radius, R_m, of the limaçon as measured from the blank centre as follows;

$$R_m = \sqrt{L^2 + 2r^2(1+\cos(2\theta))} \tag{8}$$

Equation (8) indicates that the minimum value of R_m, L, occurs at $\theta = \pi/2$ and $3\pi/2$. The maximum value of R_m is equal to $\sqrt{L^2 + 4r^2}$, and it occurs at $\theta = 0$ and π. This information is needed to allow enough material to manufacture the compression-expansion chamber.

2. MECHANICAL GENERATION

Various alternative transformations of the basic mechanism depicted in Figure (1) have been proposed by designers to produce limaçon motion suitable for fluid processing. This section is intended to demonstrate some of these mechanisms in a schematic sense, without delving into the operational details of any specific design. In every case effort will be made to identify the elements of the limaçon motion, namely, the chord and its centre point, m, the base circle, the pole, o, and the instantaneous centre, I. For the limaçon motion to be realised, m should always fall on the same base circle (along with the pole o) in order that the chord rotates at half the angular velocity of m about the circle centre. As indicated above, the instantaneous centre, I, of the chord should also fall on the base circle, diametrically opposite the rotor geometric centre, m.

Figure (3) depicts a cam-assisted mechanism first proposed by Wheildon (1896). Decades later, Georgiev (1981) introduced considerable operational improvements into the Wheildon design, but still maintained the kinematical concept on which it was built. According to this concept, the driveshaft, which is equipped with flat sliding surfaces, is located at the pole, and the chord (i.e. the lateral axis of the rotor) is allowed to slide on it. The rotor is provided with flat surfaces perpendicular to the chord, and these surfaces are allowed to slide on a stationary circular cam. By virtue of the mechanism kinematics, as Figure (3) indicates, during motion the centre of the chord stays on a circular path, the diameter of which is the distance between the driveshaft centre and the centre of the stationary cam. This circular path is the base circle of the limaçon. It is also obvious that the instantaneous centre of the chord will always fall on the base circle at a point diametrically opposite m. The mechanism will perform two compression-expansion

cycles for every single driveshaft revolution, since the axis of this shaft is made to pass by the pole, o. However, effort must be made to reduce the heat generated and losses incurred due to the use of sliding motion on round and flat surfaces. Also, such a mechanism has to be manufactured to high accuracy levels to ensure perfect roundness, parallelism and perpendicularity of different components.

Figure (4) indicates a design which utilises two perpendicular sliders as has been proposed by Feynes (1927) and Frager and Menard (1962). This is an Oldham-coupling-like mechanism which Planche (1920) has also referred to; but suggested replacing the sliders by round pins. Artobolevsky (1964) used the same mechanism (and a few of its inversions) to generate the cardioid, which is a dimpled limaçon with L set equal to 2r. The double slider mechanism will obviously produce limaçon motion since the centre of the chord, m, would always fall on a base circle along with the pole, o. The diameter of the base circle is equal to the central distance between the two slider pivots, and the driveshaft is keyed to the slider which is located at the pole, o. This design will also produce two compression-expansion cycles for every shaft revolution. The mechanism employs sliding motion on flat surfaces and is expected to exhibit mechanical losses, which can be reduced by proper bearing design and lubrication schemes. Also manufacturing accuracy would be required to ensure the perpendicularity of the sliding joint axes.

Planche (1920 and 1927) employs the straightforward fixed-centrode-moving-centrode definition, discussed above, of the limaçon to propose an epicycloidal mechanism suitable for fluid processing. The mechanism, which is described in Figure (5), consists of a ring gear allowed to rotate about a stationary gear, whose axis coincides with the driveshaft axis. The ring gear is pivoted at its centre to the end of a crank, which is, in turn, keyed to the driveshaft. The pitch circle diameter of the ring gear is twice that of the stationary gear. This ensures that the lateral axis of the rotor (which is also the, *initially*, horizontal axis of the ring gear) would have an angular velocity half that of the crank. As a result, the initial position of the ring gear centre (i.e. the pole) would always fall on the same circle (i.e. a base circle) with the moving positions of this centre (i.e.

point m). The base circle is obviously the pitch circle of the stationary gear. The mechanism depicted in Figure (5) does indeed produce limaçon motion, but the restrictions imposed on the dimensions of certain items, such as the stationary gear diameter, may end up reflecting on the dimensions of the whole machine, as per expression (5). Also for the mechanism to produce two complete compression-expansion cycles, the driveshaft has to perform two full revolutions. As such, the design produces, for the same driveshaft speed and chamber size, half the volume flow rate obtained by the embodiments, shown in Figures (3) and (4), whose rotors perform two compression-expansion cycles for every single driveshaft rotation. On the upside, the epicycloidal mechanism employs only rolling motion, excluding the sliding action on the gear teeth, and hence good mechanical efficiency may be expected.

It is worthy of noting here that both the Planche design and the Wankel-type machines employ the same epicycloidal gear train to create their respective desired motions. However, in the Wankel-type machines the ring gear has a diameter which is 3/2 that of the stationary gear. As such the horizontal axis of the ring gear rotates at 1/3, rather than 1/2, the speed of the crank; hence, the initial position of the ring gear centre and the instantaneous position of this centre do not fall on the same one circle during a full revolution. This is why the Wankel-type machines do not produce limaçon motion; instead they follow a different curve of the epitrochoidal family, the details of which may be sought in the book by Yamamoto (1981).

3. VOLUMETRIC RELATIONSHIPS

This section is intended to obtain the volumetric relationships for a limaçon-based machine similar to the one shown in Figure (2). For this purpose, Figure (6) is used to indicate an infinitesimal area, δA, of a housing sector bounded by a small arc, of the limaçon contour, and two radial rays (originated from the pole, o, and separated by an angle, $\delta\theta$). These rays represent the chord of the limaçon at positions, θ and $\theta + \delta\theta$ respectively. The infinitesimal area, δA, can be expressed as follows;

$$\delta A = \frac{1}{2} R^2 \delta\theta \tag{9}$$

where R is defined in equation (2).

The area, A_t, which falls on the topside (as shown in Figure 2) of the rotor lateral axis, can be calculated by integrating the expression (9) in the range from, θ to $\theta+\pi$. This area can, therefore, be expressed as follows;

$$A_t = \pi(r^2 + \frac{1}{2}L^2) + 4rL\cos(\theta) \tag{10}$$

The corresponding area, A_b, which falls below the rotor lateral axis, can be obtained by integrating equation (9) in the range from $\theta+\pi$ to $\theta+2\pi$. The result is as follows;

$$A_b = \pi(r^2 + \frac{1}{2}L^2) - 4rL\cos(\theta) \tag{11}$$

Equations (10) and (11) reveal that the total area, A_{tot}, enclosed by a single-loop limaçon can be calculated as follows;

$$A_{tot} = 2\pi r^2 + \pi L^2 \tag{12}$$

A_{tot} is equivalent to the area of a large circle whose centre is m and whose radius is L, added to twice the area of the base circle. Kinematically, this result indicates that the base circle has to be swept twice for the large circle, which moves in a curvilinear fashion, to be swept once by the chord. By virtue of their curvilinear motion, the horizontal and vertical axes of the large circle stay parallel to their initial directions (e.g. X and Y respectively) whilst its centre, m, rotates on the base circle.

The difference, A_{id}, between A_t and A_b is a function of the angle θ, and it can be expressed as follows;

$$A_{id} = 8rL\cos(\theta) \tag{13}$$

A_{id} is equivalent to 8 fold the instantaneous area of a triangle whose vertices are c, p1 and p2. This is a rotating triangle whose base is the limaçon chord (of length 2L) and whose variable height is equal to $r\cos(\theta)$.

The volume, V_t, available for fluid processing, above the rotor can, therefore, be calculated as follows;

$$V_t = H(\pi(r^2 + \frac{1}{2}L^2) + 4rL\cos(\theta) - A_{rotor}) \quad (14)$$

where H is the rotor longitudinal depth and A_{rotor} is half its constant cross-sectional area. Hence the corresponding volume, V_b, below the rotor may be expressed as follows;

$$V_b = H(\pi(r^2 + \frac{1}{2}L^2) - 4rL\cos(\theta) - A_{rotor}) \quad (15)$$

The volume equations (14) and (15) indicate an interesting aspect of the limaçon compression-expansion machines. The volumetric relationships of these machines are represented by simple sinusoidal expressions; consequently their other thermodynamics equations (which largely depend on these volumetric relationships) can be expressed in closed forms. The sinusoidal nature of these machines would, therefore, lend them easily to design, research and development efforts. Rosenkranz (1999) presents a study on a scotch yoke-type engine and shows how the sinusoidal disposition of such a mechanism, despite its reciprocating nature, reflects favourably on the design and operational aspects of the engine.

The maximum volume, V_{max}, of a limaçon chamber can be calculated from equation (14) as follows;

$$V_{\max} = H(\pi(r^2 + \frac{1}{2}L^2) + 4rL - A_{rotor}) \quad (16)$$

The minimum volume, V_{min}, of the chamber is calculated from equation (15) as follows;

$$V_{\min} = H(\pi(r^2 + \frac{1}{2}L^2) - 4rL - A_{rotor}) \quad (17)$$

The maximum possible volume, V_{id}, of fluid that can be induced during a suction stroke, may be used to indicate the capacity of a limaçon compression-expansion machine. This volume is simply the difference between V_{max} and V_{min}; and it can be expressed as follows;

$$V_{id} = 8rLH \quad (18)$$

which is a simple expression that depends on the limaçon parameters and the rotor depth. Expression (18) directly draws on the results of (13) above. It also suggests that the rotor area does not affect the capacity of a limaçon machine; however, this area would still reflect on the pressure characteristics and the volumetric efficiency of these machines, particularly if they were meant to handle gaseous fluids. It is worth noting here that a limaçon machine, being double-acting by nature, handles twice the value of V_{id} per each rotor revolution, barring volumetric losses due to leakage and compressibility.

In the next section a compressor will be used, as a sample application, to demonstrate the simplicity of the models which can be obtained for a limaçon compression-expansion machine.

4. SAMPLE APPLICATION - STEADY STATE COMPRESSOR PERFORMANCE

This section is intended to show the ease at which closed form models can be produced for the limaçon machines. This will be demonstrated through using a compressor by way of example, and neglecting the effects of heat transfer, speed and time dependencies. Equally simplified models would have been obtained if an expander case study had been used instead.

For a limaçon machine to be used as a compressor, inlet and discharge valves can be fitted at positions, $\theta = 0$ and $\theta = \pi$, respectively, as indicated in Figure (2). A compression stroke occurs in the chamber above the rotor and the compression ratio, C_r, can be expressed as follows;

$$C_r = \frac{\pi(r^2 + \frac{1}{2}L^2) + 4rL - A_{rotor}}{\pi(r^2 + \frac{1}{2}L^2) + 4rL\cos(\theta) - A_{rotor}} \qquad (19)$$

The instantaneous absolute pressure, P_1, can be calculated at any angle, θ, assuming isentropic compression as follows;

$$P_1 = P_i \left[\frac{\pi(r^2 + \frac{1}{2}L^2) + 4rL - A_{rotor}}{\pi(r^2 + \frac{1}{2}L^2) + 4rL\cos(\theta) - A_{rotor}} \right]^{\gamma} \tag{20}$$

where P_i, is the absolute pressure at the inlet and γ is the specific heat ratio.

The discharge valve will open at a rotor angle, $\theta = \beta$, at which the pressure would have risen to the delivery value, P_d. The angle β can be calculated by re-arranging the terms in equation (20) as follows;

$$\beta = \cos^{-1}\left[\frac{\left(\pi(r^2 + \frac{1}{2}L^2) - A_{rotor}\right)\left(\left(\frac{P_i}{P_d}\right)^{\frac{1}{\gamma}} - 1\right)}{4rL} + \left(\frac{P_i}{P_d}\right)^{\frac{1}{\gamma}} \right] \tag{21}$$

The torque, T_1, required to achieve the compression stroke can be calculated from the following relationship;

$$T_1 = P_1 \frac{dV_t}{d\theta} \tag{22}$$

When manipulated, equation (22) yields the following expression for T_1;

$$T_1 = -4rLHP_i \left[\frac{\pi(r^2 + \frac{1}{2}L^2) + 4rL - A_{rotor}}{\pi(r^2 + \frac{1}{2}L^2) + 4rL\cos(\theta) - A_{rotor}} \right]^{\gamma} \sin(\theta) \tag{23}$$

Equation (23) is valid in the range of θ, from 0 to β. The torque, T_2, required to sweep the compressed gas into the receiver, can also be calculated using the concept of equation (22), assuming that the pressure during the sweeping motion stays at the constant value of P_d. T_2 can be calculated as follows;

$$T_2 = -4rLHP_d \sin(\theta) \tag{24}$$

Equation (24) holds for the range of θ between β and π. The torque amounts calculated by equations (23) and (24) would have negative numerical values; thus confirming that

the compressor would be consuming, rather than producing, torque during the compression stroke.

During the return stroke, isentropic pressure drop will take place before the inlet valve opens. The instantaneous value of the pressure, P_2, inside the chamber during this portion of the rotor motion is given as follows;

$$P_2 = P_d \left(\frac{\pi\left(r^2 + \frac{1}{2}L^2\right) - 4rL - A_{rotor}}{\pi\left(r^2 + \frac{1}{2}L^2\right) + 4rL\cos(\theta) - A_{rotor}} \right)^{\gamma} \tag{25}$$

where θ varies from π to the angle, α, at which the inlet valve opens. This angle can be calculated as follows;

$$\alpha = 2\pi - \cos^{-1}\left[\frac{\left(\pi(r^2 + \frac{1}{2}L^2) - A_{rotor}\right)\left(\left(\frac{P_i}{P_d}\right)^{-\frac{1}{\gamma}} - 1\right)}{4rL} - \left(\frac{P_i}{P_d}\right)^{-\frac{1}{\gamma}} \right] \tag{26}$$

Once the inlet valve opens, the pressure inside the chamber can be assumed to remain equal to P_i during the suction stroke; which occupies the θ-range from α to 2π.

The shaft torque, T_3, during the isentropic expansion can be calculated in a manner similar to that described in equation (22), as follows;

$$T_3 = -4rLHP_d \left(\frac{\pi\left(r^2 + \frac{1}{2}L^2\right) - 4rL - A_{rotor}}{\pi\left(r^2 + \frac{1}{2}L^2\right) + 4rL\cos(\theta) - A_{rotor}} \right)^{\gamma} \sin(\theta) \tag{27}$$

where θ varies from π to α. The torque, T_4, which results during the induction motion, may be expressed as follows;

$$T_4 = -4rLHP_i \sin(\theta) \tag{28}$$

where θ varies from α to 2π. The torques T_3 and T_4, as produced by (27) and (28), would have positive numerical values indicating that the compressed gas would produce, rather than consume, power during the return stroke.

The volumetric efficiency, η_v, of a limaçon compressor can be obtained by subtracting V_t, as calculated at θ = α, from V_{max}, dividing the result by V_{id} and multiplying by 100. This can be written as follows;

$$\eta_v = \frac{V_{\max} - V_{\min}\left(\frac{P_d}{P_i}\right)^{\frac{1}{\gamma}}}{V_{id}} \times 100 \tag{29}$$

Equation (29) can also be expressed as a function of the delivery pressure, P_d, the limaçon parameters and half the rotor area as follows;

$$\eta_v = \left[4rL\left(\left(\frac{P_d}{P_i}\right)^{\frac{1}{\gamma}} + 1\right) - \left(\pi(r^2 + \frac{1}{2}L^2) - A_{rotor}\right)\left(\left(\frac{P_d}{P_i}\right)^{\frac{1}{\gamma}} - 1\right)\right] \times \frac{100}{8rL} \tag{30}$$

The overall pressure spectrum, P, which corresponds to a given side of the rotor, can then be expressed as follows;

$$P = \begin{cases} P_1 & for \quad 0 \le \theta < \beta \\ P_d & for \quad \beta \le \theta < \pi \\ P_2 & for \quad \pi \le \theta < \alpha \\ P_i & for \quad \alpha \le \theta < 2\pi \end{cases} \tag{31}$$

The overall fluid torque spectrum, T, which corresponds to the same side of the rotor, can also be expressed as follows;

$$T = \begin{cases} T_1 & for \quad 0 \le \theta < \beta \\ T_2 & for \quad \beta \le \theta < \pi \\ T_3 & for \quad \pi \le \theta < \alpha \\ T_4 & for \quad \alpha \le \theta < 2\pi \end{cases} \tag{32}$$

As indicated above, limaçon machines are of the double-acting type, which produces two compression-expansion cycles per a rotor revolution. This is realised by the fact that while one side of the rotor is performing a certain task (e.g. compression or expansion), the other side is performing an opposite task. Therefore, each cycle would take place on a certain side of the rotor. For the purpose of design and analysis (e.g. load calculations, power requirements and flywheel aspects), the pressure and torque spectra of the cycle which occurs on the opposite side of the rotor may be obtained by shifting the value of the angle θ by, π or $-\pi$, accordingly in the above models. The total fluid torque acting on the rotor at any angle, θ, is the algebraic sum of the torque acting on either side of the rotor.

5. NUMERICAL EXAMPLE (AIR COMPRESSOR)

The models given above for the volumetric and thermodynamic behaviour of the limaçon compressor have been used in a numerical example to prove their validity. The compressor used in the example was assigned the dimensions of r = 5 mm, L = 50 mm and H = 100 mm. As such, the capacity, V_{id}, of the compressor is 0.2 litres, per half a revolution, as obtained from equation (18). The rotor profile was taken as similar to the lower part of the limaçon, with a small clearance introduced to simulate smooth running of the machine. The inlet and delivery pressures were taken as P_{at} and 10 P_{at}, respectively, where P_{at} is the atmospheric pressure. The specific heat ratio, γ, was assigned the value of 1.4 for both the compression and return strokes.

The values of the angles β and α, which have been defined above, were calculated to be 129.9^{o} and 211^{o} respectively; and the volumetric efficiency was found to be 92.9%.

Figures (7), (8) and (9) respectively depict the pressure vs. θ, the fluid torque vs. θ and the pressure vs. volume relationships for the compressor used in the example. To plot the torque-θ curves, the values of the torque obtained from equation (32) have been multiplied by -1.

6. CONCLUSIONS

The work presented here explores the aspects of generating the limaçon curve and utilising it for fluid processing. A few attempts have been conducted over the past century to produce compression-expansion machines based on the limaçon motion, but these attempts did not culminate into industry-scale production due to replacing the proper limaçon curve by a circular one, and not giving enough attention to the profile of the rotor. With the progress made to manufacturing technology, it is expected that limaçon-based fluid processing machinery would now attract interest from the industrial community. It has been shown that machines based on the limaçon curve possess sinusoidal volumetric relationships and simplified pressure and torque equations. A sample application has been used to demonstrate the concepts discussed in the paper.

REFERENCES

1. **Artobolevsky, I. I.**, Mechanisms in Modern Engineering Design, Volume V, Part 1, Mir Publishers Moscow, 1983.
2. **Artobolevsky, I. I.**, Mechanisms for the Generation of Plane Curves, Pergamon Press Ltd, 1964.
3. **Campo, M.** Rotary Engine. US Patent No. 1310157, July 1919.
4. **Costa, S. I. R., Grou, M. A. and Figueiredo, V.** Mechanical Curves - A Kinematic Greek Look Through the Computer. Int. J. of Mathematical Education in Science and Technology, Vol. 30, No. 3, May/June 1999.
5. **Eastop, T. D. and McConkey, A.,** Applied Thermodynamics for Engineering Technologists, 5th edition, Prentice Hall, 1996.
6. **Ertesvag, I. S.** Analysis of the Vading Concept - A New Rotary-Piston Compressor, Expander and Engine Principle. Proc. Instn Mech. Engrs, Vol. 216, Part A: J. Power and Energy, 2002.
7. **Feyens, F.** Rotary Compressor. US Patent No. 1802887, July 1927.
8. **Frager, M. and Menard, H.** Rotary Volumetric Apparatus. US Patent No. 3029741, April 1962.
9. **Georgiev, G. D.** Rotary Machine with Lenticular Rotor and Circular Guide Member Therefore. US Patent No. 4300874, Nov. 1981.

10. **Hunt, K. H.** Kinematic Geometry of Mechanisms. Oxford Uni. Press, 1978.
11. **Mimmi, G. and Pennacchi, P.** Analytical Model of a Particular Type of Positive Displacement Blower. Proc. Instn Mech Engrs, Vol. 213, Part C, J. Mech. Eng. Science, 1999.
12. **Peng, X., Xing, Z., Li, L. and Shu, P.** Thermodynamic Analysis of the Rotary Tooth Compressor. Proc. Instn Mech. Engrs, Vol. 216, Part A: J. Power and Energy, 2002.
13. **Planche, B. R.** Rotary Engine or Pump. US Patent No. 1636486, July 1927.
14. **Planche, B. R.** Rotary Machine. US Patent No. 1340625, May 1920.
15. **Rosenkranz, H. G.** Simple Harmonic Piston Motion of CMCR's SYTech Engines - Influence on Design and Operation. 10th Int. Pacific Conf. on Automotive Technology, Melbourne, May 1999.
16. **Tong, S.-H. and Yang, D. C. H.** On the Generation of New Lobe Pumps for Higher Pumping Flowrate. Mech. & Mach. Theory, Vol. 35, 2000.
17. **Waldron, K. J. and Kinzel, G. L.** Kinematics, Dynamics and Design of Machinery. John Wiley and Sons Inc., 1999
18. **Wheildon, W. M.** Rotary Engine. US Patent No. 553086, Jan. 1896.
19. **Yamamoto, K.** Rotary Engine. Published by Sanaidi Co. Pty, Tokyo, 1981.

LIST OF FIGURES

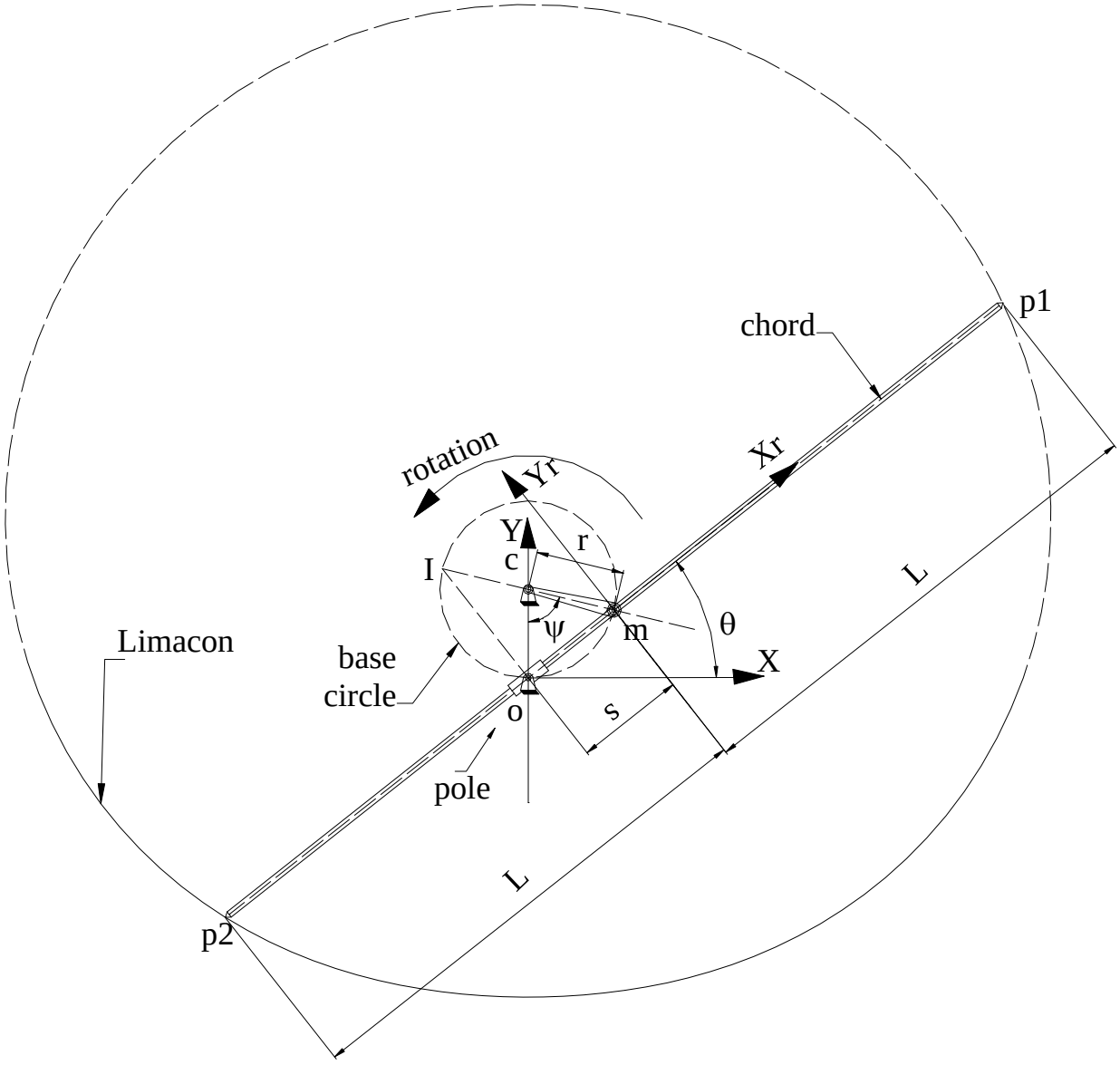

Figure (1). A mechanism to produce the limaçon motion

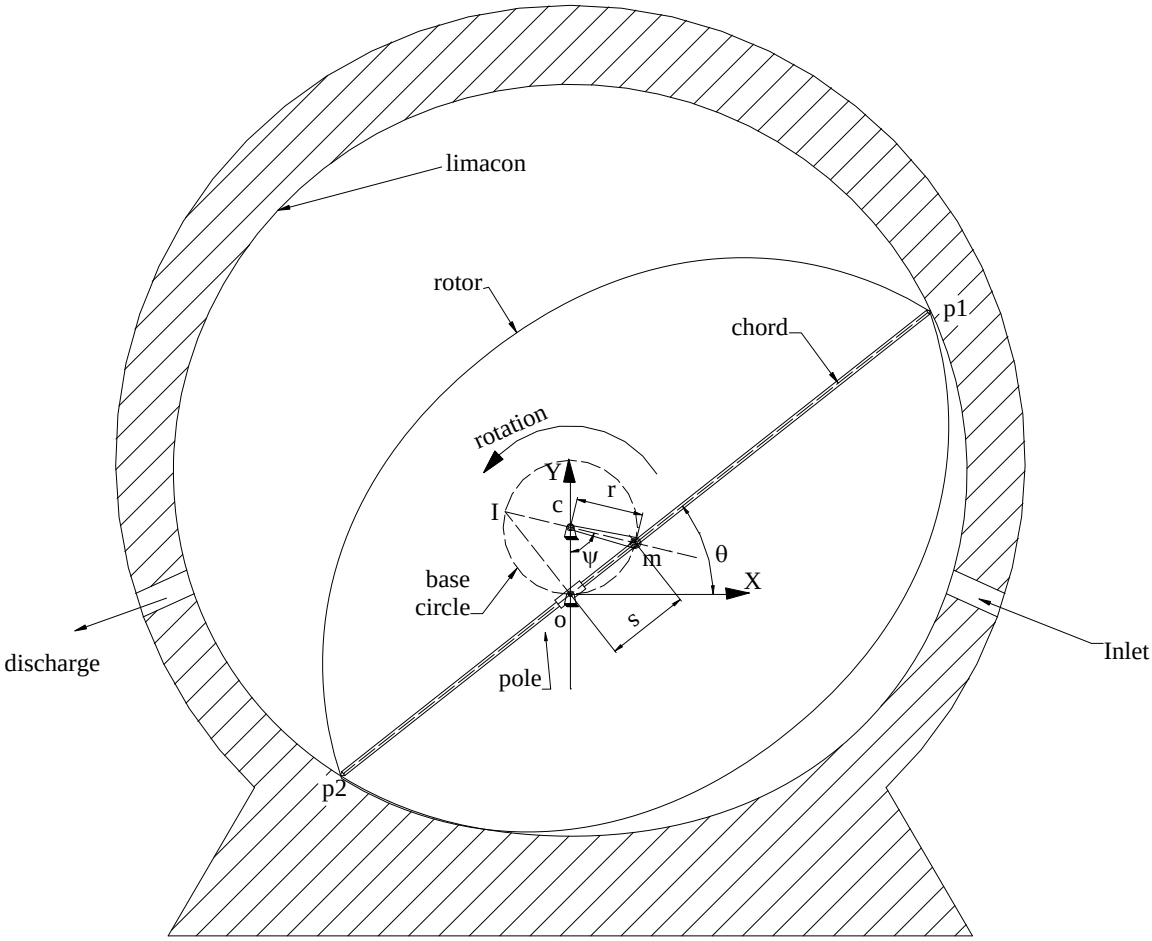

Figure (2). A limaçon mechanism employed for a compression-expansion machine.

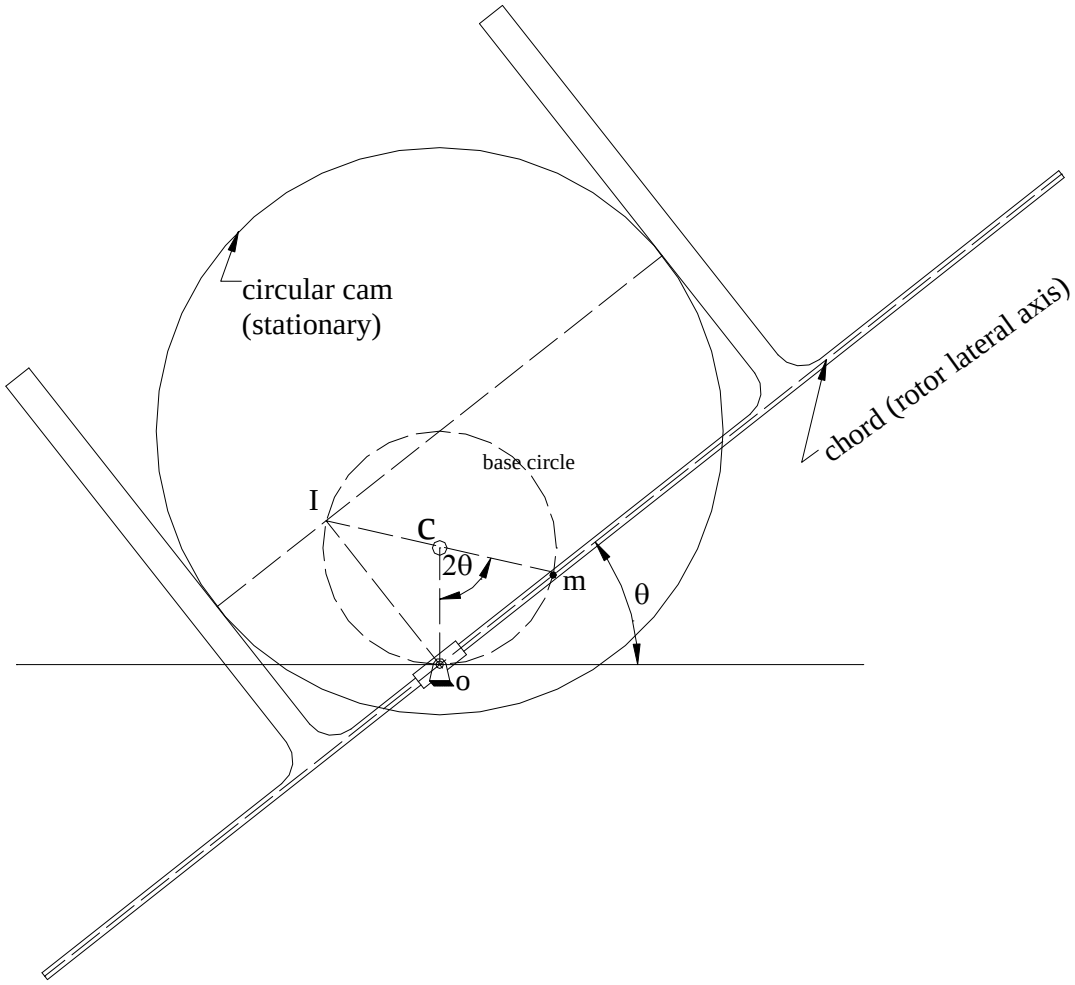

Figure (3). A cam-assisted limaçon mechanism.

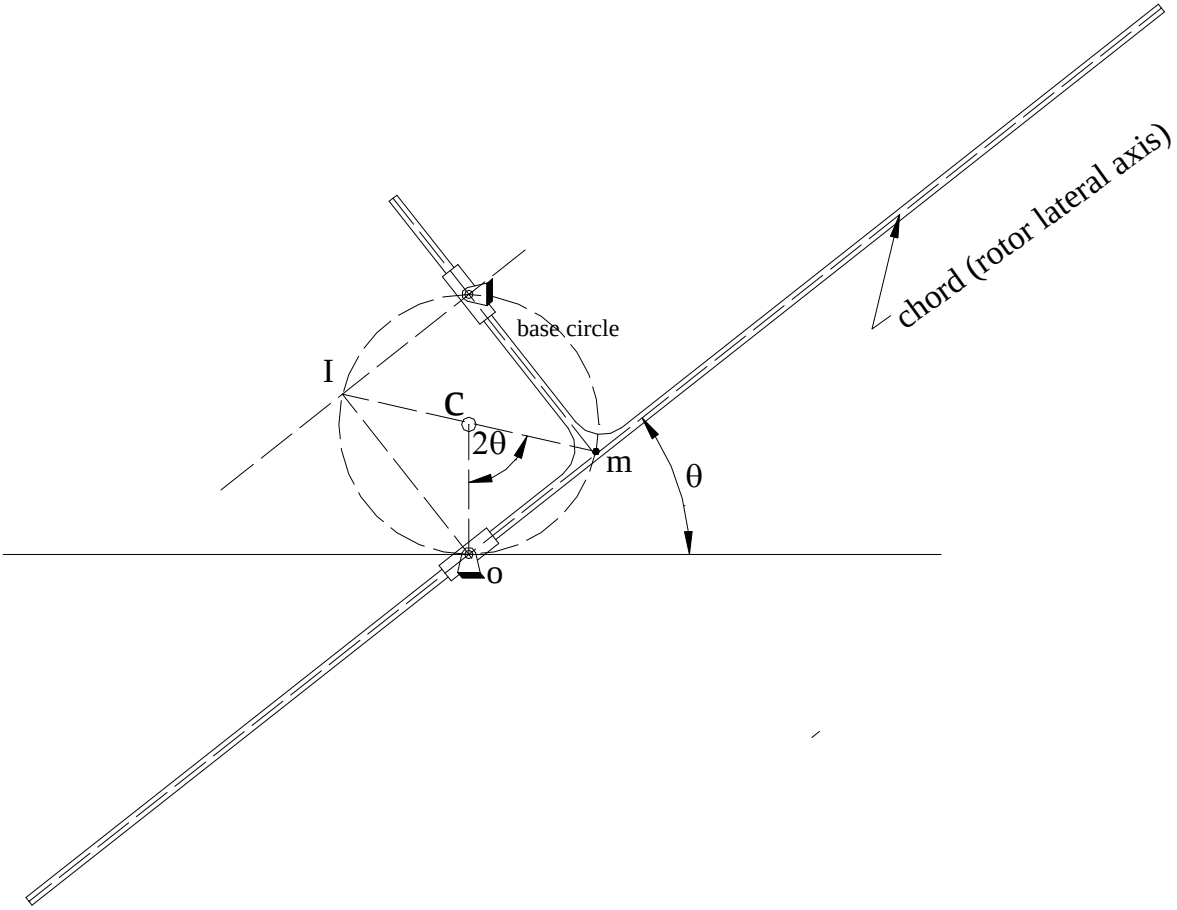

Figure (4). A double-slider limaçon mechanism.

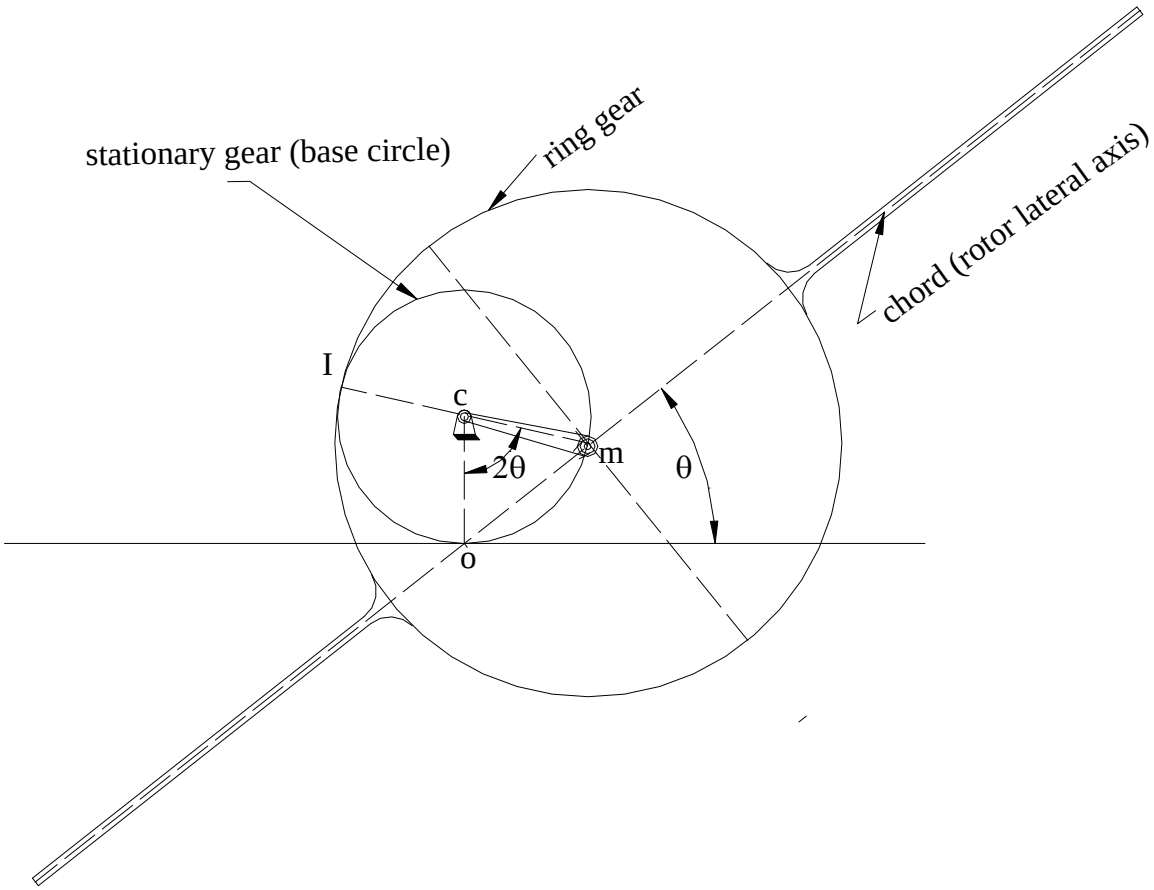

Figure (5). Generating limaçon motion with epicycloidal gears.

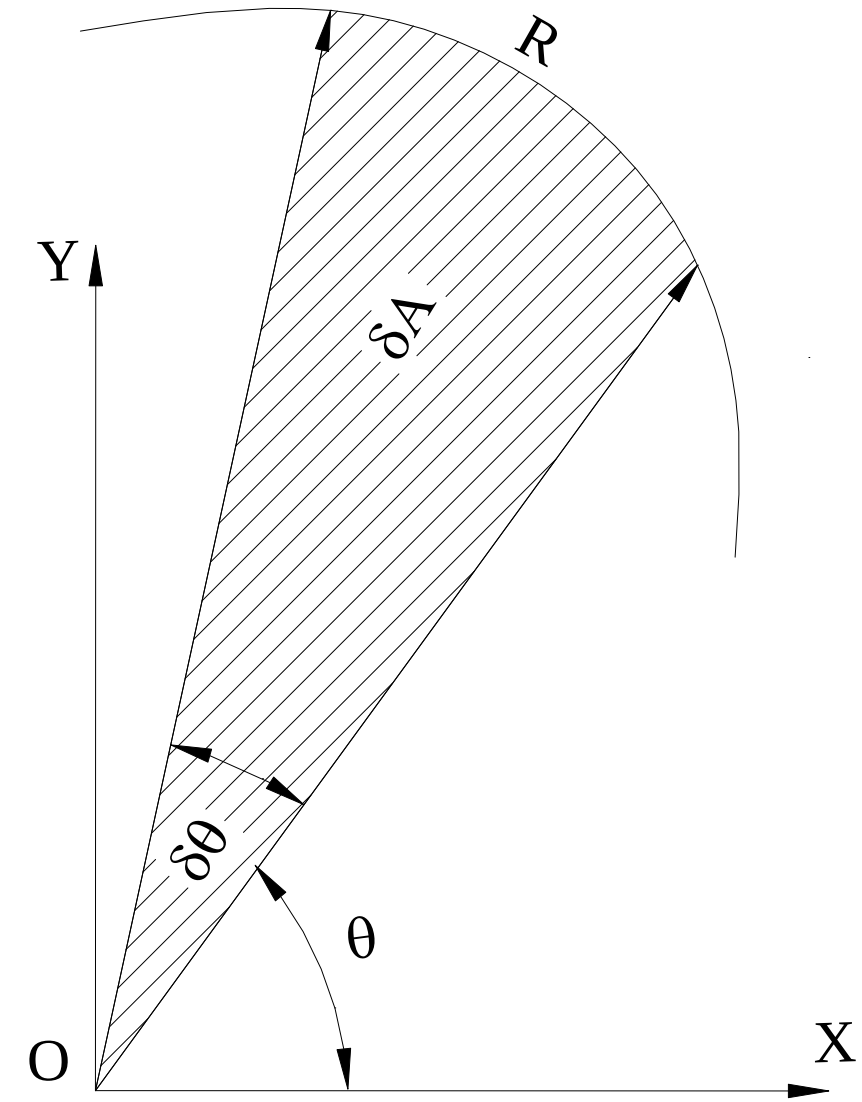

Figure (6). Area calculations.

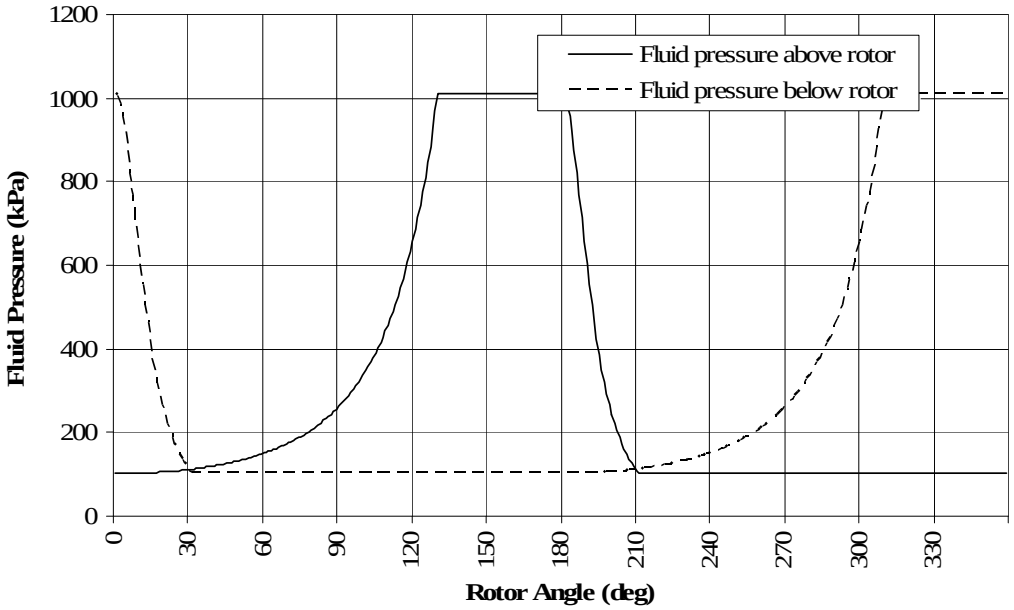

Figure (7). Pressure-θ spectrum for a limaçon compressor.

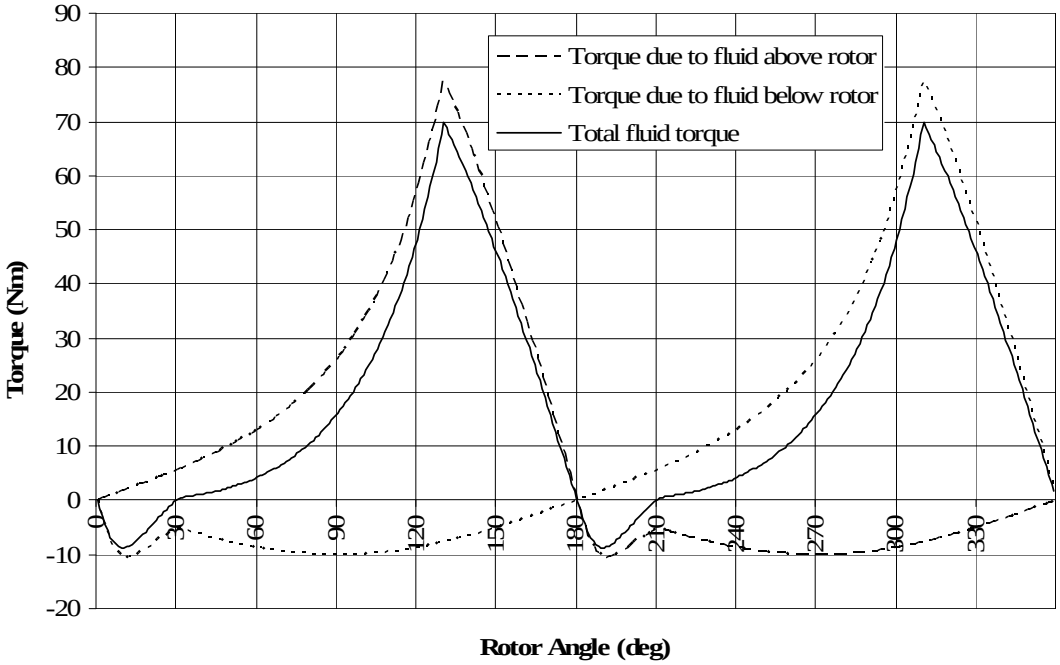

Figure (8). Torque-θ. spectrum for a limaçon compressor.

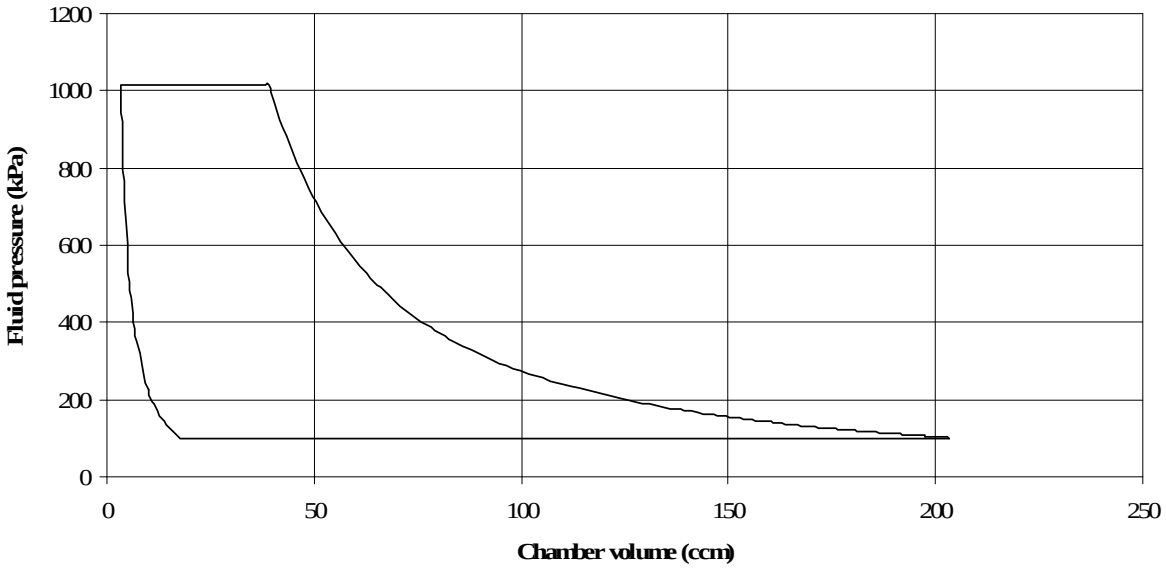

Figure (9). A PV-diagram for a limaçon compressor.